Limitations of linear control of thermal convection in a porous medium

Hui Zhao and Haim H. Bau[a)]
Department of Mechanical Engineering and Applied Mechanics, University of Pennsylvania, Philadelphia, Pennsylvania 19104

(Received 6 March 2006; accepted 30 May 2006; published online 31 July 2006)

The ability of linear controllers to stabilize the conduction (no-motion) state of a saturated porous layer heated from below and cooled from above is studied theoretically. Proportional, suboptimal robust (H_∞) and linear quadratic Gaussian (H_2) controllers are considered. The proportional controller increases the critical Rayleigh number for the onset of convection by as much as a factor of 2. Both the H_2 and H_∞ controllers stabilize the linearized system at all Rayleigh numbers. Although all these controllers successfully render negative the real part of the linearized system's eigenvalues, the linear operator of the controlled system is non-normal and disturbances undergo substantial growth prior to their eventual, asymptotic decay. The dynamics of the nonlinear system are examined as a function of the disturbance's amplitude when the system is subjected to the "most dangerous disturbances." These computations provide the critical amplitude of the initial conditions above which the system can no longer be stabilized. This critical amplitude decreases as the Rayleigh number increases. To facilitate extensive computations, we examine two-dimensional convection in a box containing a saturated porous medium, heated from below and cooled from above, as a model system. The heating is provided by a large number of individually controlled heaters. The system's state is estimated by measuring the temperature distribution at the box's midheight. All the controllers considered here render the linearized, controlled system's operator non-normal. The transient amplification of disturbances limits the "basin of attraction" of the nonlinear system's controlled state. By appropriate selection of a controller, one can minimize, but not eliminate, the controlled, linear system's non-normality.
[DOI: 10.1063/1.2221354]

I. INTRODUCTION

In recent years, there has been a growing interest in developing control strategies to alter the behavior of fluids. Much of the work to date has focused on turbulence control and drag reduction in shear flows.[1–5] There are, however, many materials processing applications in which the naturally occurring flow patterns are not optimal for the process at hand and a controller would allow operation under more optimal conditions than the naturally occurring ones. For example, convection in low Prandtl number fluids such as liquid metals readily becomes time dependent. Since the microscopic growth rate of a crystal is sensitive to the temperature oscillations generated by oscillatory flow,[6] the resulting crystal may not be homogeneous. Indeed, Kuroda *et al.*[7] have demonstrated that the density of crystal microdefects increases monotonically as a function of the amplitude of the fluid's oscillations. Carruthers *et al.*[8] and Müller *et al.*[9] have shown that compositional variations, such as doping striations in the crystals, can be generated by unsteady, convective flow in the melt. Thus, suppression of convection in the melt and/or removal of oscillatory convection may significantly improve the quality and economics of the production of single crystal materials. Clearly, there is considerable interest in devising control strategies for convective systems.

Early work[10–16] has focused on controlling convection in thermal convection loops. This system has the advantage of being amenable to low-dimension modeling. Proportional,[10–12] optimal,[13,16] nonlinear,[14] and neural network[15] controllers were used in experiment and theory to suppress chaotic advection in a thermal convection loop.

Tang and Bau[17–22] and Howle[23–26] demonstrated in theory and experiment that similar ideas can be extended to systems with a large number of degrees of freedom such as the Rayleigh-Bérnard (hereafter referred to as RB) problem of a horizontal fluid layer heated from below and cooled from above. In the RB problem, as long as the Rayleigh number is smaller than a critical value Ra_0, the motionless conduction state is globally stable. In the above, Ra_0 denotes the critical number for the onset of convection in the absence of a controller. Tang and Bau and Howle used *ad hoc* proportional controllers to delay the transition from the motionless to the motion state. In other words, with the aid of a controller, they increased the critical Rayleigh number for the onset of convection from Ra_0 to Ra_C, where Ra_C denotes the critical Rayleigh number of the controlled system. The theory predicts that the critical Rayleigh number can be increased by as much as a factor of 10 (i.e., $\mathrm{Ra}_C = 10\,\mathrm{Ra}_0$). Unfortunately, a much more modest level of stabilization was observed in the experiments. Shortis and Hall[27] studied theoretically the use of a combination of linear and nonlinear controllers to prevent the occurrence of subcritical bifurcations in non-Boussinesq fluids.

More recently, Or *et al.*[28,29] used synthesis methods such

[a)]Author to whom correspondence should be addressed. Electronic mail: bau@seas.upenn.edu

as a linear quadratic Gaussian (LQG or H_2) controller to demonstrate that the system can be stabilized at any desired Rayleigh number. The synthesis method is an optimization-based technique that allows one to devise a proportional controller to stabilize the system at a particular Rayleigh number Ra_D, to which we refer as the design Rayleigh number. Unfortunately, the LQG controller that is designed to operate at Ra_D can stabilize the system only for a range of Rayleigh numbers $\mathrm{Ra}_D^{\mathbf{L}} < \mathrm{Ra}_D < \mathrm{Ra}_D^U$. When $\mathrm{Ra}_D > 14.5\,\mathrm{Ra}_0$, $\mathrm{Ra}_D^L > 0$.[29] In other words, when $\mathrm{Ra}_D > 14.5\,\mathrm{Ra}_0$, the controlled system is not robust. No information was provided on Ra_D^L and Ra_D^U as functions of Ra_D.

Another factor that may adversely affect a linear controller's robustness is the system's nonlinearities (unmodeled dynamics). To investigate the ability of linear controllers to cope with finite amplitude disturbances, Tang and Bau[22] and Or and Speyer[29] integrated numerically the nonlinear equations with initial conditions corresponding to steady, finite amplitude convection and demonstrated that the controller can suppress established convection and bring the system to a motionless state. To obtain rigorous estimates of the basin of attraction of the controlled state, one may construct an appropriate Lyapunov ("energy") function and determine the regions of phase space in which the Lyapunov function decays with time. For the low-dimensional case of the thermal convection loop,[16] the phase space was divided into two regions: one in which the Lyapunov function decays and another in which it increases. Matters were complicated, however, by the fact that trajectories crossed from one region to the other. Although it was possible to identify an ellipsoid in phase space within which the Lyapunov function decayed monotonically, the corresponding estimates of stability were extremely conservative.

The difficulty arises in part because the operator of the linearized, controlled system is non-normal. The term non-normal is used here to imply that even when all the linear operator's eigenvalues have a negative real part and all the disturbances of the linear system are guaranteed to decay asymptotically, the decay may, however, not be monotonic.[30–33] Indeed, when the system is non-normal, certain disturbances may amplify greatly before eventually decaying, thereby rendering the nonlinear (neglected) terms important and providing a bypass mechanism for the subcritical transition from one state to another state.[34] We will show that the non-normality of the linear operator of the controlled system increases as the Rayleigh number increases and that this trend adversely affects the stability of the nonlinear system.

The increased non-normality of the linear operator of the controlled system as a parameter (i.e., the Reynolds number) increases was previously demonstrated by Lauga and Bewley,[35] who studied the stability of the controlled, linear, complex Ginzburg-Landau model of spatially developing flow. When the non-normality of the controlled system's linear operator exceeded a certain threshold, it became impossible to compute the control algorithms needed to stabilize the linear system.[35] In essence, Lauga and Bewley[35] addressed the important issue of the computability of linear control algorithms. In a companion paper, Lauga and Bewley[36] demonstrated that a linear, robust controller can stabilize the nonlinear complex Ginzburg-Landau equation for Reynolds $\mathrm{Re} < 97$.

The Rayleigh numbers considered in this paper are sufficiently small to allow the computation of the linear controller that stabilizes the linearized system, and we do not encounter similar difficulties to the ones encountered by Lauga and Bewley.[35] Also, our focus is different. We investigate the effect of non-normality on the stability of the nonlinear system.

To facilitate extensive computations, we carry out our numerical study focusing on the two-dimensional Lapwood problem of convection in a box containing a saturated porous medium, heated from below and cooled from above.[18] This system has many similarities with the RB problem, but is less demanding to study in terms of computational resources. The heating is provided by a large number of individually controlled heaters, which are located along the bottom of the layer similar to the arrangement used in our experimental apparatus.[21] The system's state is estimated by measuring the temperature distribution at the box's midheight. To stabilize the motionless state, we design various controllers, ranging from an *ad hoc* proportional controller, to a LQR (H_2) controller, to a suboptimal robust (H_∞) controller. We demonstrate that in the absence of actuator constraints, the *ad hoc* proportional controller can increase the critical Rayleigh number for the onset of convection by a factor of 2 ($\mathrm{Ra}_C \sim 2\,\mathrm{Ra}_0$). In contrast, both the H_2 and the H_∞ controllers can stabilize the system at any desired Rayleigh number. The H_2 and H_∞ controllers designed to stabilize the system at a particular Ra_D, are effective only for a range of Rayleigh numbers $\mathrm{Ra}_D^{\mathbf{L}} < \mathrm{Ra}_D < \mathrm{Ra}_D^U$. We compute Ra_D^L and Ra_D^U as functions of Ra_D for both the H_2 and H_∞ controllers. Next, we investigate the normality of the controlled system's linear operator, and we identify the vectors that amplify the most. We refer to these vectors as the "most dangerous" ones. Finally, by numerical simulation, we compute the response of the nonlinear system to the "most dangerous" disturbances and obtain the largest amplitude of the disturbance at which the controller can still stabilize the nonlinear system as a function of the Rayleigh number.

II. MATHEMATICAL MODEL

Consider a two-dimensional square box with edge length H, filled with a saturated porous medium. The insulated sidewalls of the box are parallel to the gravity vector. The box is heated from below with a specified heat flux. The heating is provided by individually controlled heaters. In the absence of control, all the heaters are set to supply a uniform flux q_0. In the presence of a controller, the heat flux given by the various heaters is $q_0[1+q(x,t)]$, where $q(x,t)$ may vary both temporally (t is time) and spatially (x). An array of sensors, positioned inside the box, monitors the temperature distribution in the saturated porous medium and provides an input to the controller. The relationship between q and the temperatures in the interior of the box are defined by the control strategy. The box's top is maintained at a uniform temperature T_0.

Hereafter, we use dimensionless quantities. $0 \leqslant x \leqslant 1$ is the horizontal coordinate, and $-0.5 \leqslant y \leqslant 0.5$ is the vertical coordinate. The box's edge length H is the length scale. The dimensionless mass conservation (continuity), momentum (Darcy's law), and energy equations are,[37] respectively,

$$\nabla \cdot \mathbf{V} = 0, \tag{1}$$

$$\mathbf{V} = -\nabla P + \mathrm{Ra}\, T e_y, \tag{2}$$

and

$$\chi \frac{\partial}{\partial t} T + \mathbf{V} \cdot \nabla T = \nabla^2 T. \tag{3}$$

The boundary conditions are as follows: impermeable walls,

$$n \cdot \mathbf{V} = 0; \tag{4}$$

insulated side walls,

$$n \cdot \nabla T(0,y) = n \cdot \nabla T(1,y) = 0; \tag{5}$$

constant temperature top wall,

$$T(x,0.5) = 0; \tag{6}$$

and heat flux at the bottom surface,

$$n \cdot \nabla T(x,-0.5) = 1 + q(x,t). \tag{7}$$

In the above, e_y is the unit vector in the vertical direction; $\mathbf{V}$ is the velocity vector with components v_x and v_y; T is the temperature; P is the pressure; $\mathrm{Ra} = g\lambda\beta H^2 q/\nu\alpha\kappa$ is the Darcy-Rayleigh number; g is the gravitational acceleration; λ is the permeability; ν is the fluid's kinematic viscosity; β is the thermal expansion coefficient; α and κ are, respectively, the saturated medium's apparent thermal diffusivity and conductivity; and χ is the ratio between the equivalent thermal capacity of the medium and that of the saturating fluid. H^2/α is the time scale; α/H is the velocity scale; Hq_0/κ is the temperature scale; and T_0 is the reference temperature.

Equations (1)–(7) admit the motionless state ($\mathbf{V}=0$, $T=0.5-y$). This is a fixed point of the dynamic system for all Rayleigh numbers. The motionless state is stable only when $\mathrm{Ra} < \mathrm{Ra}_0 \sim 27.1$. Our objective is to devise control strategies to delay the transition to the motion state. In other words, we wish to increase the magnitude of Ra_0.

Since we will use linear control theory, we write below the linearized form of Eqs. (1)–(3) in local form about the motionless state:

$$\chi \frac{\partial}{\partial t} \theta = \nabla^2 \theta + v_y \tag{8}$$

and

$$\nabla^2 v_y = \mathrm{Ra} \frac{\partial^2 \theta}{\partial x^2}. \tag{9}$$

In the above, θ is the deviation of the temperature from its no-motion, conductive value.

In what follows, we will resort to numerical techniques. We reduce Eqs. (8) and (9) to a set of ordinary differential equations using finite elements with triangular elements and linear shape functions:[38,39]

$$\chi D_a \dot{\Theta} = -K_2 \Theta + Lq + C_1 V_y \tag{10}$$

and

$$K_1 V_y = \mathrm{Ra}\, P_1 \Theta. \tag{11}$$

In the above, Θ and V_y are vectors consisting, respectively, of the temperatures and vertical velocities at various nodal points; and q is the control variable representing the heat flux deviation from its nominal value. The coefficients are matrices. By eliminating V_y in favor of θ, the system (10) and (11) reduces to the form of a plant equation (the terminology is borrowed from control theory):

$$\dot{X}(t) = A(\mathrm{Ra})X(t) + B_u U(t) + B_w w(t) \tag{12}$$

and

$$Y(t) = CX(t). \tag{13}$$

In the above, the dependent variables Θ (state variables) are denoted $X(t)$; $Y(t)$, the temperature deviation in the midplane, is the observed (measured) signal; $w(t)$ represents disturbances (white noise in the case of the H_2 controller and worst disturbance in the case of the H_∞ controller); and $U(t)$ is the control input (q). In most of our calculations, we set B_w equal to the identity matrix. In some cases, we used $B_w = B_u$. Recall that Eqs. (12) and (13) are written in local form, i.e., $X = U = 0$ is an equilibrium state. Due to the difference in the nature of the boundary conditions at the layer's top (Dirichlet) and bottom (Neuman), the operator A is not self-adjoint. Our objective is to stabilize this equilibrium state for the time interval $0 < t < t_f$. Below, we will focus on the case when t_f is large (infinity).

To verify the numerical code, we computed the eigenvalues of the operator A as functions of the Rayleigh number and determined the critical Rayleigh number at which the real part of the largest eigenvalue crosses from a negative to a positive value. When 371 elements were used, the computed critical Rayleigh numbers for the uncontrolled problem (Neuman boundary condition) and for the related problem of a fixed bottom temperature (Dirichlet boundary condition) were, respectively, 29.3 and 37.1. These are in good agreement with published data.[40] The number of elements that were used in the actual calculations was increased as the Rayleigh number increased. When $\mathrm{Ra} < 200$ and $\mathrm{Ra} > 200$, we used, respectively, 371 and 734 elements. The sufficiency of the selected number of elements was established by obtaining comparable results with different numbers of elements. For example, when $\mathrm{Ra} = 470$, the leading eigenvalues of the linear operator computed with 734 and 1116 elements agreed within 1.5%.

III. CONTROL STRATEGIES

We will explore three different control strategies: *ad hoc* proportional, H_2, and H_∞. The hardware associated with the controller can be implemented in various ways. For example, Tang and Bau[21] constructed a cylindrical cell in which the heated surface consisted of a large number of individually controlled heaters and an array of sensors was positioned at the cylinder's midheight. Howle[23] constructed an experimen-

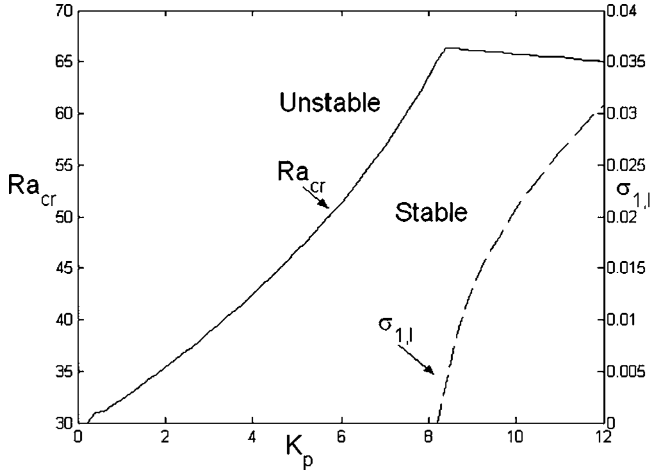

FIG. 1. The critical Rayleigh number (solid line) for the transition from the motionless to the motion state and the corresponding imaginary part σ_I of the largest eigenvalue (dashed line) are depicted as functions of the *ad hoc* proportional controller gain K_p.

tal apparatus that consisted of a rectangular box, in which a shadowgraph was used to measure the average liquid density along the height of the box as a function of location.

A. *Ad hoc* proportional controller

The *ad hoc* proportional controller of the type used by Tang and Bau[17] is the simplest to implement and the most intuitive. In this control strategy, the control input (the heat flux at $y=-0.5$) is modulated in proportion to the deviation of the midlayer temperature from its conductive value

$$U=-K_pX(x,0,t), \tag{14}$$

where K_p is the scalar controller's gain. In other words, each sensor communicates with a single actuator. To determine the control capacity, we investigate the linear stability of the controlled system by calculating the eigenvalues of the linear operator $(A-B_uK_p)$. We denote the largest eigenvalue of $(A-B_uK_p)$ as $\sigma_1=\sigma_{1,R}+i\sigma_{1,I}$. For different values of the controller's gain (K_p), we compute the Rayleigh number and $\sigma_{1,I}$ that corresponds to $\sigma_{1,R}=0$. Figure 1 depicts the critical Rayleigh number Ra_c of the controlled system (solid line) and the imaginary part of the eigenvalue ($\sigma_{1,I}$, dashed line) as functions of the controller gain. The regions under and above the solid line correspond, respectively, to stable (S) and unstable (U) states. As K_p increases, the critical Rayleigh number increases as well. When $K_p=8.4$, the critical Rayleigh number is about 66.8. When $K_p<8.4$, the bifurcation from the no-motion to the motion state occurs through a simple eigenvalue ($\sigma_{1,I}=0$). When $K_p>8.4$ the bifurcation occurs through a complex pair of eigenvalues ($\sigma_{1,I}\neq 0$, Hopf bifurcation), and the resulting supercritical motion is oscillatory. Further increases in the controller's gain reduce the critical Rayleigh number. Although this reduction can be avoided with a proportional-derivative controller, we do not explore this control strategy here.

To postpone the transition from the no-motion to the motion state to even higher Rayleigh numbers, we use the tools of optimal control theory.[41] The basic idea is to identify a controller that optimizes an appropriate objective or cost function.

B. H_2 controller

As a measure of the system's performance, we define the positive, quadratic cost function:

$$J[X(t),U(t)]=\lim_{t_f\to\infty}\frac{1}{t_f}\int_0^{t_f}(X^TQX+l^2U^TRU)dt, \tag{15}$$

where Q and R are weights that allow one to adjust the relative importance of the various outputs and the cost of the control. The choice of the objective function is not unique. The task is to determine a controller $U(t)$ that minimizes the cost function (15) with the plant equation (12) serving as a constraint. Below, we select the identity matrices for the weights Q and R. We used the parameter l to allow us to easily adjust the relative importance of the various terms in (15) without a need to vary Q and R. In most of the paper, we provide results when $l=1$. In Sec. IV, we will examine the effect of l on the normality of the controlled system's linear operator.

Using the standard techniques of variational calculus and introducing the Lagrange multipliers $p(t)$, we convert the minimization problem to the corresponding Euler-Lagrange equations (referred to as the Hamiltonian system). Upon introducing the linear relationship between the Lagrange multipliers and the state variables $p(t)=P(t)\times X(t)$, the problem is reduced to the solution of the nonlinear, matrix differential equation (the Riccati equation):

$$\frac{dP}{dt}=PA+A^TP-PB_uB_u^TP+Q. \tag{16}$$

The optimal feedback controller is

$$U(t)=-l^{-1}R^{-1}B_u^TPX(t)=-KX(t), \tag{17}$$

where $K(t)$ is the gain matrix. When $t_f\to\infty$, $K(t)$ approaches asymptotically a time-independent value.

Witness that implementation of the controller (17) requires full knowledge of all state variables, but typically just a few state variables are available for observation. Hence, in order to implement the controller, it is necessary to construct an estimator (filter) capable of estimating the system's state variables.

The plant estimator equation is

$$\dot{\hat{X}}(t)=A\hat{X}(t)+B_uU+G(m-C\hat{X}), \tag{18}$$

where the superscript wiggle denotes state estimates; $m(t)$ is the measured (observed) signal; and G is the filter's gain. The optimal (Kalman) filter gain is found by minimizing the appropriate quadratic cost function that is proportional to the difference between the predicted and measured observations.[41] The procedure for determining the optimal filter gain G is analogous to the calculation of the H_2 optimal controller gain.

The controlled plant [Eqs. (12) and (17)] together with the estimator (18) constitute the dynamic system

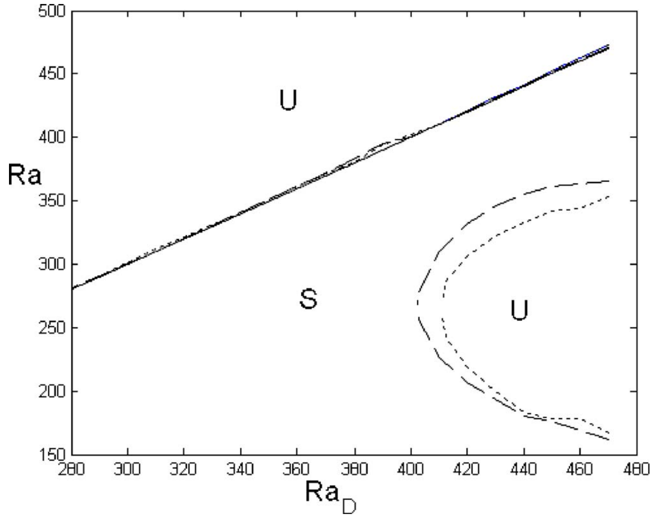

FIG. 2. The range of Rayleigh numbers for which the controlled system is stable as a function of the Rayleigh number for which the controller was designed (Ra_D). The solid line depicts the design Rayleigh number. The dashed and dotted lines correspond, respectively, to the linear, quadratic Gaussian controller (H_2) and the suboptimal robust controller (H_∞). The regions of stability and instability are indicated in the figure with the letters S and U, respectively.

$$\dot{\tilde{X}}(t) = A_c \tilde{X}(t), \tag{19}$$

where

$$\tilde{X}(t) = \begin{Bmatrix} X(t) \\ \hat{X}(t) \end{Bmatrix}, \quad A_c = \begin{pmatrix} A & -B_u K_p \\ GC & A - B_u K_p - GC \end{pmatrix}.$$

In contrast to the *ad hoc* proportional controller, the H_2 optimal controller is capable of stabilizing the linear system at any desired Rayleigh number. In other words, theoretically, at any Rayleigh number Ra_D, it is possible to design a controller that would render the linear system stable. An interesting question is whether a controller designed to stabilize the system at $\mathrm{Ra}=\mathrm{Ra}_D$ can stabilize the system when operating at Rayleigh numbers other than the one for which it was designed. This issue of controller robustness is addressed in Fig. 2. In Fig. 2, the horizontal and vertical axes correspond, respectively, to the design Rayleigh number Ra_D and the actual Rayleigh number Ra at which the system operates. The solid line is a 45° line. The dashed and dotted lines provide, respectively, the range of the Rayleigh numbers for which the system is stable when the H_2 and the H_∞ (next subsection) controllers are used. Witness that once the design Rayleigh number Ra_D exceeds a certain value ($\mathrm{Ra}_D > 402$), the controller no longer can stabilize the system for all $\mathrm{Ra} < \mathrm{Ra}_D$. A controller designed to stabilize the system at $\mathrm{Ra}=\mathrm{Ra}_D$ can stabilize the system only when $\mathrm{Ra}_D^U > \mathrm{Ra} > \mathrm{Ra}_D^L$.

When $\mathrm{Ra}_D < 402$, the controller can stabilize the system for all $\mathrm{Ra} < \mathrm{Ra}_D^U$. Since the cost function accounts for the cost of the control, it is not surprising that the upper stability margin Ra_D^U is tight and close to the design value. For example, the H_2 optimal controller designed to stabilize the linear system at $\mathrm{Ra}=330$ is capable of stabilizing the system only as long as $\mathrm{Ra} < 331$.

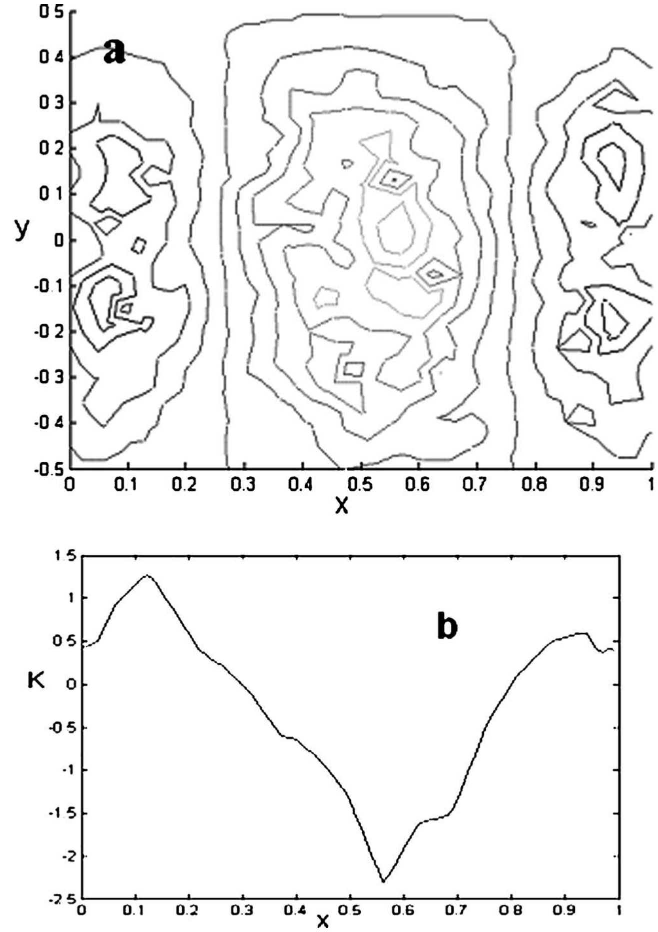

FIG. 3. Contours of the H_2 controller gain associated with an actuator located at $x=0.6$ are depicted as a function of location (a) and $K(x,0)$ is depicted as a function of x (b). The controller is designed to operate at $\mathrm{Ra}_D=120$.

When $\mathrm{Ra}_D > 402$, $\mathrm{Ra}_D^L > 0$. As Ra_D increases, the stable region shrinks, and an unstable island appears in the region $\mathrm{Ra} < \mathrm{Ra}_D$, as indicated by the dashed line in Fig. 2. The size of the unstable island increases as the Ra_D increases. Figure 2 provides limitations on the structural robustness of the H_2 optimal controller. Nevertheless, the H_2 controller significantly outperforms the *ad hoc* proportional controller (Sec. III A).

Another interesting issue is the relative importance of the various state variables to the controller's function. We surmise that the state variable associated with the largest controller gains would be the most critical for the controller's function. It would be desirable then to install the sensors at the most critical locations. To this end, Fig. 3(a) depicts the contours of the gain $K(x,y;0.6)$ associated with the actuator located at $x=0.6$ as a function of spatial location (x,y) when $\mathrm{Ra}_D=120$. The figure depicts multiple peaks, suggesting that the controller requires information from multiple locations rather than just a few ones. Figure 3(b) depicts $K(x,0)$ as a function of x. In the *ad hoc* control strategy, the actuator located at $x=0.6$ was controlled by data supplied by a sensor located at $(x,y)=(0.6,0)$. Although in the H_2 control strategy, $|K(x,0)|$ attains its maximum near $x=0.6$, significant controller gains are associated with other spatial locations.

Finally, when studying the control of the linear Ginzburg-Landau equation, Lauga and Bewley[35] observed that the Ricatti equation could be solved only when the Reynolds number was smaller than a certain threshold value. Above the threshold value, they found it impossible to compute linearly stabilizing control algorithms. In the range of Rayleigh numbers considered here ($\mathrm{Ra} \leqslant 470$), we did not encounter any difficulties in computing control algorithms. It is likely that in our case the threshold of the type described in Lauga and Bewley[35] is larger than $\mathrm{Ra}=470$ (the largest Rayleigh number considered in this paper).

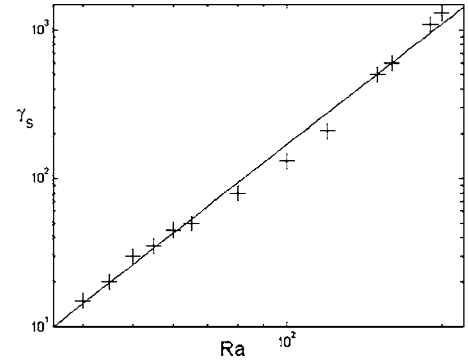

FIG. 4. The smallest bound γ_s of the H_∞ transfer function for which a steady solution of the Riccati equation exists as a function of the Rayleigh number.

C. H_∞ controller (robust controller)

The objective of the suboptimal H_∞ control problem is to find a controller for the plant [Eqs. (12) and (13)] such that the transfer function

$$\sup_{w(t)} \frac{\|Z(t)\|_2}{\|w(t)\|_2} < \gamma \tag{20}$$

is bounded. In the above, $\|\cdot\|_2$ denotes the L_2 norm $\|Z(t)\|_2^2 = \int_0^{+\infty} X^T(t) Q X(t) dt$ and γ is a constant. One would like γ to be as small as possible. Time-independent solutions of the control problem may exist only when γ is larger than some threshold value. The solution of Eq. (20) is equivalent to finding the saddle point of the objective function[41]

$$J_1 = \|Z(t)\|_2^2 - \gamma^2 \|w(t)\|_2^2 + l^2 \|U(t)\|_2^2. \tag{21}$$

In other words, one attempts to compute the controller that minimizes the objective function J_1 in the presence of the worst possible disturbances $w(t)$. In the above, l is a weight that allows one to adjust the cost of the control. In the following, we used $l=1$. Similar to the case of the H_2 controller, Eq. (21) can be reduced to a Riccati matrix equation. Upon solving this Riccati equation, one obtains the suboptimal H_∞ feedback controller:[41]

$$U(t) = -KX(t). \tag{22}$$

Like the H_2 optimal controller, the suboptimal controller H_∞ requires full information about the plant's state. To this end, we replace the state variable in Eq. (22) with the estimated one. The state estimates are calculated by solving the estimator equations (18) with a suboptimal H_∞ filter G.[41]

The performance of the suboptimal H_∞ controller depends critically on the magnitude of the bound γ. When $\gamma \to \infty$, the suboptimal H_∞ controller gain is identical to the optimal H_2 controller gain. The smallest possible γ value that facilitates a real (noncomplex) solution for the Ricatti equation was determined by trial and error. Figure 4 depicts the smallest possible γ, γ_s, as a function of the Rayleigh number. γ_s increases nearly exponentially as the Rayleigh number increases, $\gamma_s \sim e^{-7.3}\,\mathrm{Ra}^{2.7}$. When γ is relatively large, we would expect little difference between the H_2 and H_∞ controllers. This expectation is supported by Fig. 2, where we depicted the stability margins of the controlled system as a function of the design Rayleigh number Ra_D. The dotted line depicts the stable regions associated with the suboptimal H_∞ controller. Witness that the stable regions are just slightly larger than those afforded by the optimal H_2 controller. For example, the suboptimal H_∞ controller maintains linear stability for all $\mathrm{Ra} < \mathrm{Ra}_D$ as long as $\mathrm{Ra}_D < 410$, while the optimal H_2 controller provides a similar measure of stability only when Ra_D is smaller than 402.

IV. THE NORMALITY OF THE CONTROLLED SYSTEM'S LINEAR OPERATOR

In the previous section, we showed that the various controllers render the real part of the system's eigenvalues negative and assure asymptotic stability for Rayleigh numbers far exceeding the critical one in the controller's absence. In other words, the controllers assure that all disturbances eventually decay, albeit not necessarily monotonically. It is possible, however, for disturbances to amplify (sometimes a great deal) before their eventual decay. Stable linear systems in which all the disturbances decay monotonically are known as normal. When this is not the case, the system is dubbed non-normal.[30–33] For example, self-adjoint (symmetric) operators are always normal. When the eigenvectors are not orthogonal, they may interact to produce a substantial transient growth before eventual decay, and the system is said to be non-normal.

Transient growth of disturbances is undesirable since large disturbances may render the neglected nonlinear terms important, thus providing a bypass mechanism for transition from the stabilized state to another state. Moreover, since any system is continuously subjected to noise, non-normal systems, even when controllable, will operate away from the desired equilibrium state—a state of affairs coined linear turbulence.[42] Finally, non-normality may adversely affect the computability of the control algorithm.[35] Hence, it is important to assess the effect of various control strategies on the normality of the linear operator.

The normality of an operator is evaluated by examining its pseudospectra.[32] Briefly, consider the linear operator A_c. Let ΔA_c be a perturbation to A_c such that $\|\Delta A_c\|_2 = \varepsilon \|A_c\|_2$. The ε pseudospectra of A_c, $\Lambda(A_c,\varepsilon)$, is the set of eigenvalues z_ε of $A_c + \Delta A_c$. When A_c is normal, then $\Lambda(A_c,\varepsilon)$ is a set of points within a distance ε from the corresponding points in $\Lambda(A_c,0)$. When A_c is non-normal, the distance between points in $\Lambda(A_c,\varepsilon)$ and the corresponding points in $\Lambda(A_c,0)$.

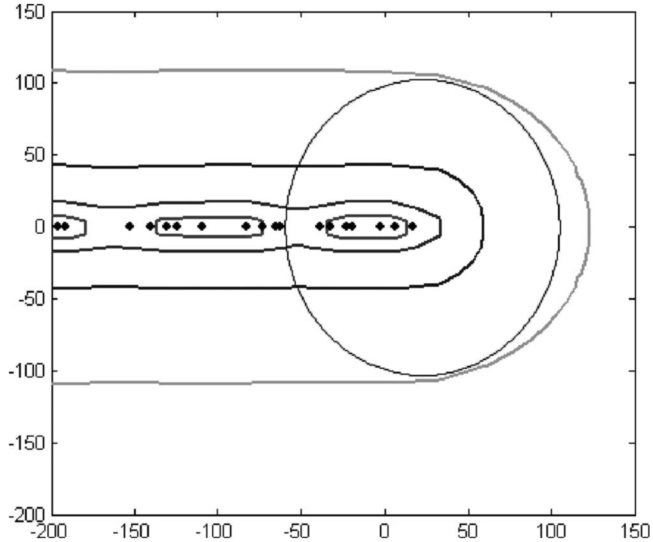

FIG. 5. The pseudospectra of the linear operator A of the uncontrolled system when Ra=66. The contour lines correspond to $\varepsilon=1$, $10^{1/2}$, 10, $10^{3/2}$, and 10^2. The disk has a radius of 100.

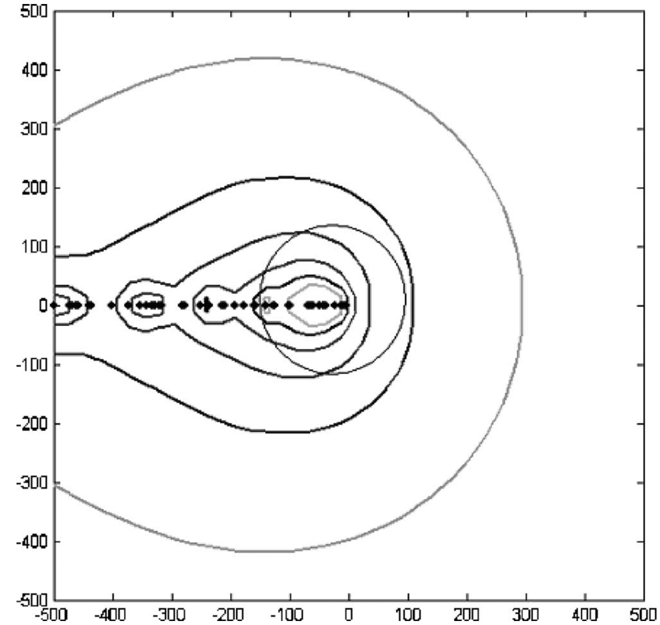

FIG. 6. The pseudospectra of the linear operator A_c of the system controlled with an *ad hoc* proportional controller when Ra=120. The contour lines correspond to $\varepsilon=1$, $10^{1/2}$, 10, $10^{3/2}$, and 10^2. The disk has a radius of 100.

will be much larger than ε. We computed the pseudospectra of the controlled and uncontrolled systems. Figure 5 depicts the locus of the eigenvalues of the uncontrolled system when Ra=66 and $\varepsilon=0$, $10^{1/2}$, 10, and 100. The horizontal and vertical axes correspond, respectively, to the real and imaginary parts of the eigenvalues. When $\varepsilon=0$, all the eigenvalues are real and located on the real axis. Since the system is not stable, some of the eigenvalues are positive. The largest eigenvalue is encircled with circles of radii $\varepsilon=10^{1/2}$, 10, and 100. Witness that the largest eigenvalue of $\Lambda(A_c,\varepsilon)$ lies within the disk of radius ε. The same is true for all the other eigenvalues. Although the operator A_c is asymmetric, it is nearly normal. Unfortunately, this is not necessarily true for the operators associated with the controlled system. Figure 6 depicts the ε pseudospectra associated with the H_2 controller when Ra=120. The disk has a radius of 100. Witness that the eigenvalues $\Lambda(A_c,\varepsilon)$ lie outside the disk, which is consistent with a non-normal operator.

The linear controlled system admits a formal solution of the form

$$\tilde{X}(t)=\exp[A_c t]X(0), \tag{23}$$

where $X(0)$ represents the initial perturbation at time $t=0$. Accordingly, $\|\tilde{X}(t)\|=\|\exp(A_c t)\tilde{X}(0)\|$, where $\|\tilde{X}(t)\|^2=\tilde{X}^T(t)\tilde{X}(t)$. Hence,

$$G(t)=\sup_{\tilde{X}(0)}\frac{\|\exp(A_c t)\tilde{X}(0)\|}{\|\tilde{X}(0)\|} \tag{24}$$

is a measure of the disturbance's growth. When the operator A_c is normal, $G(t)$ will decrease monotonically as t increases. When the operator is non-normal (albeit stable), $G(t)$ will initially increase and eventually asymptotically decay as t increases.[30] To illustrate the basic idea, Fig. 7 depicts $G(t)$ as a function of time (t) for the proportional controller with gain $K_p=8.4$ and Ra=66. Witness that initially $G(t)$ increases, attains a maximum value of about 8 at $t=t_{\max}\sim 0.6$, and then eventually decays to zero. We define the maximum value of $G(t)$,

$$G_{\max}=\max_{0\leqslant t\leqslant\infty} G(t), \tag{25}$$

and use it as a measure of the disturbance's amplification.

Figure 8 depicts $G_{\max}$ as a function of Ra for the *ad hoc* proportional controller ($K_p=8.4$, solid line), the H_2 controller with state estimator (dashed line, $B_w=I$), the H_2 controller without estimator when all state variables are measured (dotted line), and the suboptimal H_∞ controller (dashed-dotted line). Figure 8(a) spans the range of low Rayleigh numbers ($40<\text{Ra}<66.6$) and allows a clearer comparison between the *ad hoc* proportional and the H_2 and H_∞ controllers. Figure 8(b) spans a larger range of Rayleigh numbers: $40<\text{Ra}<200$. The solid line terminates at Ra=66.8 since this is the largest Rayleigh number at which the *ad hoc* proportional controller can stabilize the system. Figure 8 illustrates that $G_{\max}$ increases as the Rayleigh number increases. The $G_{\max}$ associated with the *ad hoc* proportional controller undergoes the most rapid (nearly exponential) increase as the Rayleigh number increases. Not surprisingly, the $G_{\max}$ associated with the suboptimal H_∞ controller is the smallest at almost all

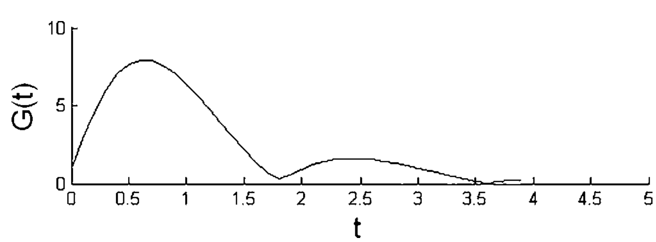

FIG. 7. The transient growth of the system as a function of time. *Ad hoc* proportional controller, Ra=66, and $K_p=8.4$.

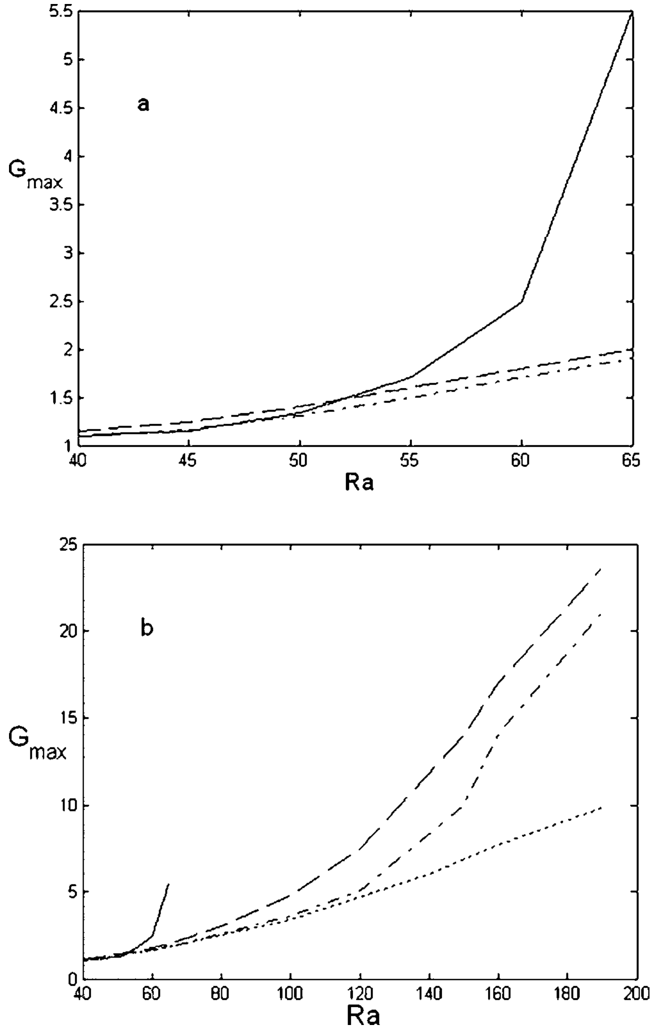

FIG. 8. The maximum transient growth $G_{\max}$ as a function of the Rayleigh number for the various control strategies. The solid, dashed, and dashed-dotted lines correspond, respectively, to the *ad hoc* proportional (with gain $K_p=8.4$), quadratic-Gaussian (H_2), and suboptimal robust (H_∞) controllers.

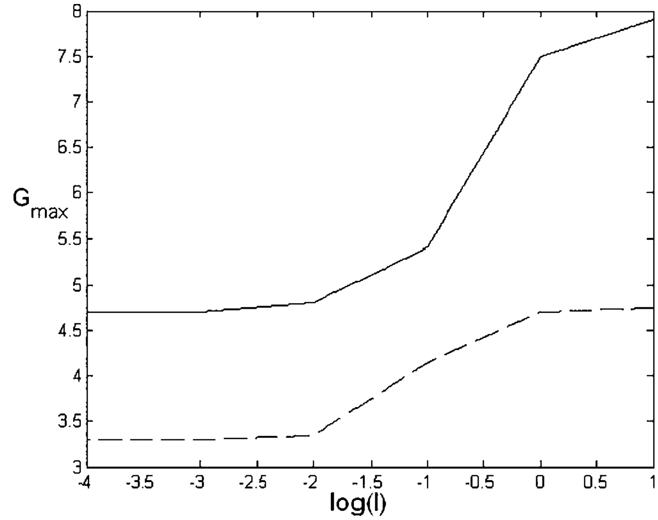

FIG. 9. The maximum transient growth $G_{\max}$ as a function of the relative weight l. The solid and dashed lines correspond, respectively, to the H_2 controller with a state estimator and the H_2 controller without a state estimator. Ra=120.

Rayleigh numbers. This is because the suboptimal H_∞ controller synthesis takes into account the worst possible disturbances. Witness that $G_{\max}$ when full state information is available [dotted line, Fig. 8(b)] is smaller than $G_{\max}$ in the presence of the state estimator. Both the controller and the state estimator contribute to the non-normality. Interestingly, at low Rayleigh numbers (Ra<50), the *ad hoc* proportional controller appears to perform better than the H_2 and H_∞ controllers (with state estimators). This is because the *ad hoc* controller does not require a state estimator. Indeed, when we assumed that the full state information was available to the H_2 controller, the $G_{\max}$ of the optimal controllers decreased below the one associated with the *ad hoc* proportional controller. In conclusion, as the Rayleigh number increases, so does the non-normality of the linear operator of the controlled system. To examine the effect of B_w on the controller's performance, following Or *et al.*,[28] we set $B_w=B_u$. The results were nearly identical to the case of $B_w=I$.

We repeated the calculations with different weights l in the H_2 objective function [Eq. (15)]. Figure 9 depicts $G_{\max}$ as a function of the weight l when Ra=120. The solid and dashed lines correspond, respectively, to the H_2 controller with state estimator and the H_2 controller without estimator (when all the state information is available). In both cases, the curve has a "sigmoid" shape that assumes asymptotic values for small and large l. As the weight l increases from 10^{-4} to 1, $G_{\max}$ increases from ~4.7 to 7.9 (in the presence of the state estimator) and from ~3.3 to 4.7 when full state information is available. The figure indicates that both the controller and the estimator contribute to the non-normality of the controlled system and that even when full state information is available, the controlled system is still non-normal. Although variations in l affected the numerical value of $G_{\max}$, they did not affect the qualitative nature of the results.

In the control literature, transfer function norms are often used to characterize the effect of disturbance on the controlled system. We take the Laplace transform of the controlled system (including the estimator) to obtain the transfer function (T_{yw}) from the disturbance $w(s)$ to the output $y(s)$:

$$y(s) = \tilde{C}(sI - \tilde{A})\tilde{B}w(s) \equiv T_{yw}(s)w(s). \tag{26}$$

Two different transfer function norms are commonly used: 2-norm,

$$\|T_{yw}\|_2^2 \equiv \int_{-\infty}^{+\infty} \mathrm{trace}[T_{yw}(j\omega)^* T_{yw}(j\omega)]d\omega \tag{27}$$

and ∞-norm,

$$\|T_{yw}\| \equiv \sup_{\omega} \sigma_{\max}[T_{yw}(j\omega)] \text{ with } \sigma_{\max} \equiv \text{maximum singular value}. \tag{28}$$

Following the algorithm described in Bewley and Liu,[4] we calculated both the 2-norm and ∞-norm. Figures 10(a) and 10(b) depict, respectively, the 2-norm and the ∞-norm as functions of the Rayleigh number. The solid and dashed lines correspond, respectively, to the H_2 and H_∞ controllers. Not surprisingly, the norm of the transfer function associated

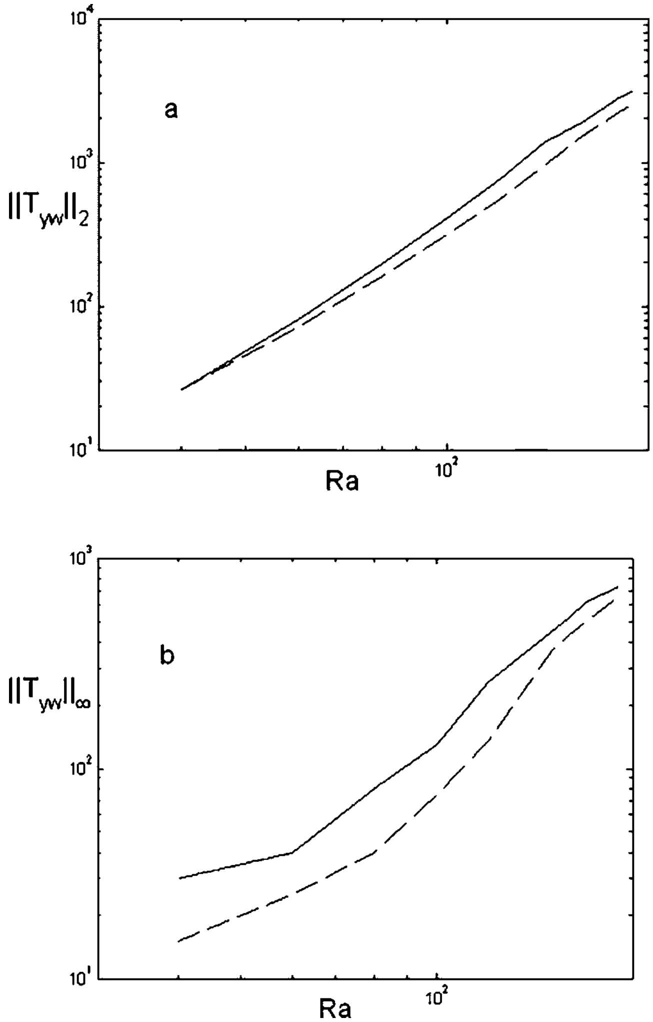

FIG. 10. The transfer function norms: (a) 2-norm, (b) ∞-norm as functions of the Rayleigh number. The solid and dashed lines correspond, respectively, to quadratic-Gaussian (H_2) and suboptimal robust (H_∞) controllers.

with the H_∞ controller is somewhat smaller than the one associated with the H_2 controller. Qualitatively, the trends depicted in Fig. 10 are similar to the ones observed in Fig. 8 and reported by Lauga and Bewley[35] for a different system. As the Rayleigh number increases, the non-normality of the linear operator of the controlled system increases and so do the various norms of the transfer functions. $G_{\max}$ and the norms of the transfer functions can be crudely approximated as functions of the Rayleigh number of the form $C\,\mathrm{Ra}^m$, where $2 < m < 3$.

The non-normality of the linear operator of the controlled system raises a concern about the basin of attraction of the controlled state, a concern that we address in the next section.

V. DYNAMICS OF THE NONLINEAR CONTROLLED SYSTEM

Thus far, we have dealt solely with the linearized plant and neglected the system's nonlinearities. Next, we will study the dynamics of the controlled, nonlinear system. We wish to estimate the basin of attraction of the controlled state. Rigorous determination of the basin of attraction requires the construction and investigation of the appropriate Lyapunov function. Such an investigation is far from trivial, if at all feasible. Instead, we assume that the "most dangerous" disturbance is the one that leads to the maximum transient growth, i.e., the disturbance that corresponds to $G_{\max}$. Singular value decomposition[34] allows us to determine this "most dangerous" disturbance.

Briefly,

$$U^H \exp(A_c t_{\max}) V = \sum , \tag{29}$$

where U and V are unitary matrices with orthogonal columns ($UU^H = V^H V = I$) and Σ is a diagonal matrix that contains the singular values. The singular values are the square roots of the eigenvalues of $\exp(A_c t_{\max})^T \exp(A_c t_{\max})$. We arrange the singular values in descending order with σ_1 being the largest singular value. V_1 and U_1 are, respectively, the corresponding right and left singular vectors. Multiplying Eq. (29) on the left with U, we have

$$\exp(A_c t_{\max}) V = U \sum \tag{30}$$

and

$$\exp(A_c t_{\max}) V_1 = U_1 \sigma_1 . \tag{31}$$

In other words, when the system is subjected to the initial condition $x(0) = V_1$, it yields the state $\sigma_1 U_1$ at time $t = t_{\max}$. Among all the disturbances of norm 1, V_1 is the disturbance that leads to the maximal amplification. To see this, witness that

$$\|\exp(A_c t_{\max})\| = \sigma_1 = G_{\max} . \tag{32}$$

We subjected the nonlinear system to a disturbance of magnitude εV_1, integrated the ODEs [Eqs. (12) and (18)], and followed the transient as a function of ε. Our objective is to find, at each Rayleigh number, the largest value of ε at which the nonlinear, controlled system is still stabilized. We denote this critical value as ε_c.

In the numerical simulations, we used 371 linear elements, a third-order Runge-Kutta integration scheme in time, an implicit scheme for the viscous term,[43] and an explicit scheme for the nonlinear terms. To verify the code, we calculated the temperature and velocity distributions of the uncontrolled system at sub- and supercritical Rayleigh numbers, reproducing known results and obtaining favorable agreement with the predictions of linear stability analysis.

Figure 11 illustrates the process of identifying ε_c as a function of Ra. We prescribe a Ra number and synthesize a controller for the same Rayleigh number. We then specify an initial condition of the form εV_1, where V_1 is the right singular vector corresponding to the linear operator of the controlled system and integrate the nonlinear system. The temperatures and velocities at various spatial locations are recorded as a function of time. For example, the conditions of Fig. 11 correspond to a system controlled with a proportional controller with a gain $K_p = 8.4$ and Ra=66. The figure depicts the temperature at the point $(x,y) = (1/8, 0)$ located at midheight. When $\varepsilon = 0.07 < \varepsilon_c$ [Fig. 11(a)], the initial disturbance decayed to the desired steady (set) state of 0.5. When $\varepsilon = 0.08 > \varepsilon_c$ [Fig. 11(b)], the system moved to a different,

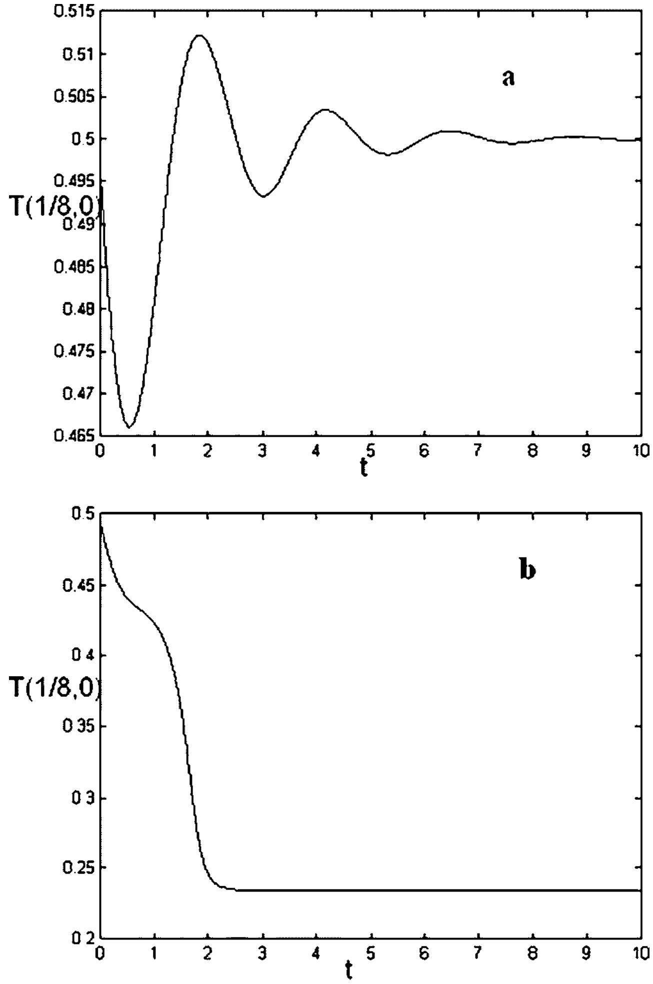

FIG. 11. The temperature T at $(x,y)=(1/8,0)$ is depicted as a function of time. *Ad hoc* proportional controller, Ra=66, and $K_p=8.4$. The disturbance amplitude is, respectively, 0.07 and 0.08 in (a) and (b).

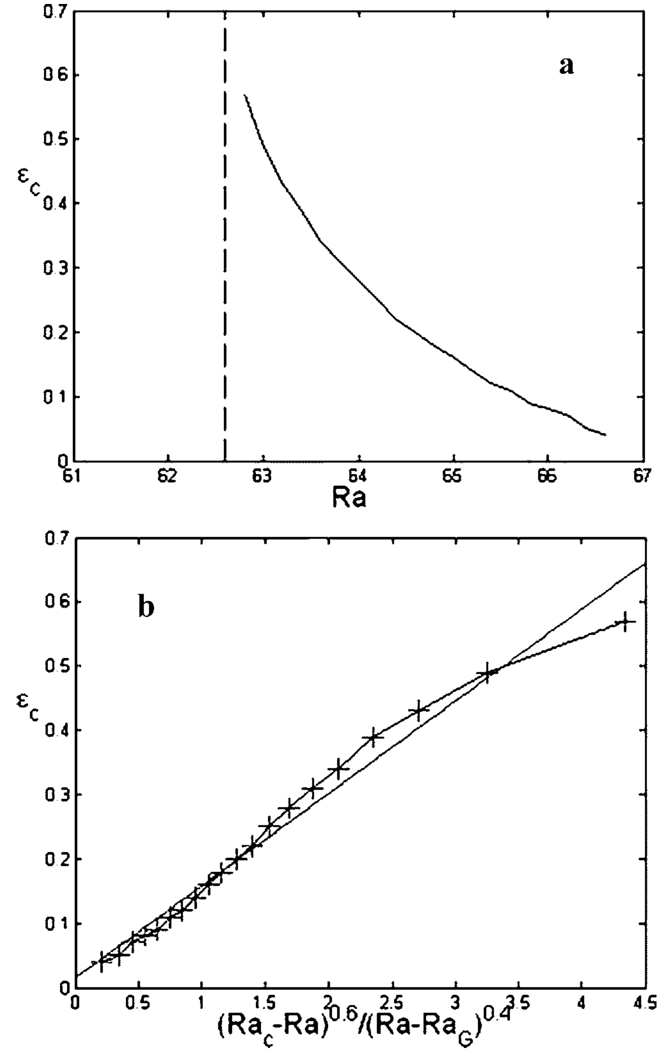

FIG. 12. The critical disturbance amplitude ε_c defining the basin of attraction of the controlled state as a function of the Rayleigh number (a) and as a function of $(\mathrm{Ra}_c-\mathrm{Ra})/(\mathrm{Ra}-\mathrm{Ra}_G)^{0.6}$ (b). *Ad hoc* proportional controller. $K_p=8.4$.

undesirable steady state. By carrying out a few additional simulations in the range $0.08>\varepsilon>0.07$, we estimated ε_c. Since these simulations are very time consuming, we carried out a systematic study only for the proportional controller and the H_2 controller.

The results of these investigations are summarized in Fig. 12. Figure 12(a) depicts ε_c as a function of the Rayleigh number. In Fig. 12(a), we used the *ad hoc* proportional controller with a gain $K_p=8.4$. The critical Rayleigh number Ra_C of the controlled system was 66.8. When $\mathrm{Ra}<\mathrm{Ra}_G\sim 62.6$, all disturbances decayed regardless of the magnitude of ε. Recall that the uncontrolled Lapwood problem is globally stable when $\mathrm{Ra}<\mathrm{Ra}_0$. Hence, in the uncontrolled problem, $\mathrm{Ra}_G=\mathrm{Ra}_0$. This is no longer true in the controlled system. The controller successfully increased the magnitudes of both Ra_c and Ra_G. In Fig. 12(a), the controller increased Ra_G to ~ 62.6 while Ra_c was increased to 66.8. We speculate that the controlled system is globally stable when $\mathrm{Ra}<\mathrm{Ra}_G$. When $\mathrm{Ra}>\mathrm{Ra}_G$, the magnitude of ε_c decreases exponentially as Ra increases until ε_c shrinks to zero at $\mathrm{Ra}=\mathrm{Ra}_C$. Thus, in the range $\mathrm{Ra}_G<\mathrm{Ra}<\mathrm{Ra}_C$, the controlled system is conditionally stable. As long as the disturbance's amplitude is not too large, the controller successfully stabilizes the system. Once the amplitude has exceeded a certain critical value ε_c, the controller is no longer able to suppress the disturbance.

Figure 12(b) summarizes the data presented in Fig. 12(a) in a slightly different way. The figure depicts ε_C as a function of $(\mathrm{Ra}_c-\mathrm{Ra})^{0.6}/(\mathrm{Ra}-\mathrm{Ra}_G)^{0.4}$. The symbols and solid line represent, respectively, the results of the numerical simulations and a best-fit curve. Witness that the data is nearly distributed about a straight line and ε_c can be correlated as

$$\varepsilon_c \approx 0.14\frac{(\mathrm{Ra}_c-\mathrm{Ra})^{0.6}}{(\mathrm{Ra}-\mathrm{Ra}_G)^{0.4}} \quad (\mathrm{Ra}_G<\mathrm{Ra}<\mathrm{Ra}_C). \tag{33}$$

Similar qualitative behavior is exhibited by systems controlled with the suboptimal H_∞ and H_2 controllers. Figure 13 depicts the critical amplitude of the "most dangerous disturbance" when the H_2 controller is employed. The symbols correspond to the results of numerical computations. The solid lines connect the data points for better visibility. When Ra=125, the critical amplitude $\varepsilon_c\sim 0.02$. As the Rayleigh number decreases, the critical amplitude increases, achieving a value of $\varepsilon_c\sim 0.68$ at Ra=95. When Ra is decreased below

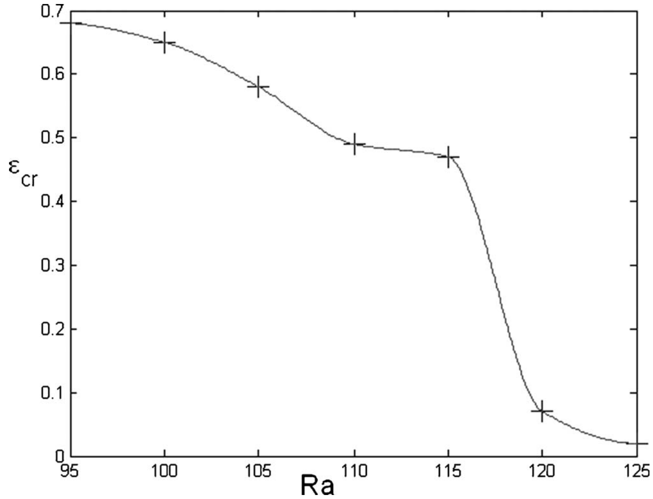

FIG. 13. The critical amplitude of the optimal disturbance as a function of the Rayleigh number Ra for the H_2 optimal controller.

90, we are not able to identify the critical amplitude for loss of stability of the H_2 controlled system. Clearly, the H_2 controller not only stabilizes the system at significantly larger Rayleigh numbers than the *ad hoc* proportional controller does but also provides a much larger "basin of attraction." The H_∞ controller does even better. When Ra=125, $\varepsilon_c \sim 0.1$.

VI. CONCLUSIONS

In this paper, we studied the use of linear proportional, quadratic Gaussian, and suboptimal H_∞ controllers to stabilize the no-motion state of the Lapwood problem. The Lapwood problem was selected for study as a model problem because it exhibits complex physical behavior similar to the Rayleigh Benard problem in the range of Rayleigh numbers considered here and it allows us to carry out a fairly extensive computational study in a reasonable amount of time.

The *ad hoc*, linear, proportional controller is capable of increasing the critical Rayleigh number for the transition from the no-motion state to the motion state by as much as a factor of 2. Since the plant is stable and detectable, the synthesized suboptimal H_∞ and quadratic Gaussian regulators H_2 do not have any limitations in terms of the magnitude of the Rayleigh number. In other words, in theory, they are capable of stabilizing the no-motion state at any desired Rayleigh number. In our case, there appears to be little difference between the performance characteristics of the quadratic Guassian H_2 and the suboptimal H_∞ controllers.

There are, however, various practical considerations that may limit the ability of the controllers considered here to stabilize the linearized system. For instance, our analysis assumed that the actuator's output is unconstrained. In practice, the actuator is likely to saturate when the control signal is too large, which may limit the controller's ability to stabilize the system. The magnitude of the control signal depends on the magnitude of the disturbances.

Our study reveals that the linear operator of the controlled system is non-normal. The non-normality as well as the norms of the transfer function increase rapidly (exponentially) as the Rayleigh number increases. These observations are consistent with those of Lauga and Bewley,[35] who reported that the operator of the nonlinear, complex Ginzburg-Landau equation becomes increasingly non-normal as the Reynolds number increases. Although detailed calculations have been carried out only for a very few systems, the above results may have broad implications about the linear controllers' ability to control the nonlinear system and about the computability of control algorithms at moderate and large systems' parameters (Reynolds or Rayleigh numbers).

The increasing non-normality of the linear operator implies that disturbances may amplify a great deal before eventual decay. Such amplification may lead to an actuator's saturation and may adversely impact the controller's ability to suppress disturbances. Moreover, large disturbances render the neglected nonlinear terms important. These terms were not accounted for in the controller design process. Numerical experiments reveal that the controlled state's basin of attraction depends on the magnitude of the Rayleigh number. When the Rayleigh number is sufficiently small, the system is globally stable. As the Rayleigh number increases, the size of the basin of attraction decreases. It appears that in order to overcome some of the above shortcomings, one needs to construct a controller that minimizes the system's non-normality. Alternatively, some of the above-discussed limitations may be removed with a nonlinear controller.

An interesting question is whether the non-normality of the controlled, linear system arises from poor design of the linear controller or it is an intrinsic property of the controlled system. Our study clearly indicates that the non-normality can be reduced with appropriate controller design. Recently, Whidborne *et al.*[44] have proposed a convex optimization algorithm to design an optimal, dynamic feedback controller that minimizes transient growth of disturbances. Unfortunately, the non-normality of the controlled linear system cannot be eliminated altogether. To demonstrate that this is, indeed, the case, we apply Whidborne's theorem[44] to the system (12) and (13) and set $B_w=0$. Briefly, the existence of a controller of the form $u=Ky$ that causes all disturbances to decay monotonically requires that the following conditions hold:

$$B^{\perp}(A+A^T)B^{\perp T} < 0 \quad \text{or} \quad BB^T > 0 \tag{34}$$

and

$$C^{T\perp}(A+A^T)C^{T\perp T} < 0 \quad \text{or} \quad C^T C > 0. \tag{35}$$

In the above, $B^{\perp}$ and $C^{\perp}$ denote, respectively, the left null spaces of the matrices B and C. We consider the special case of all the state variables being available for observation $C=I$. The second part of the second condition (35) is automatically satisfied. The second part of the first condition (34) is not satisfied and for the controlled system to be normal, we check whether the first condition is valid. To this end, we calculate the largest eigenvalue $\lambda_{\max}$ of the matrix $B^{\perp}(A+A^T)B^{\perp T}$. Figure 14 depicts $\lambda_{\max}$ as a function of the Rayleigh number. Witness that $\lambda_{\max}>0$ and increases as the Rayleigh number increases. Hence, we conclude that all linear controllers of the system (12) and (13) induce non-

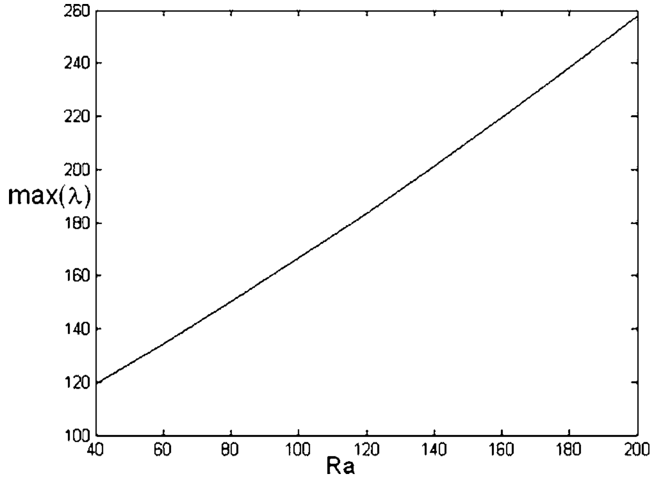

FIG. 14. The maximum eigenvalue of the system $B^{\perp}(A+A^{T})B^{\perp T}$ as a function of the Rayleigh number (Ra).

normality and that the non-normality (the transient growth) increases as the Rayleigh number increases.

ACKNOWLEDGMENTS

The work was supported, in part, by the National Science Foundation Grant No. CTS-0212998 to the University of Pennsylvania. We are grateful to the anonymous reviewers for valuable comments.

[1] H. Hu and H. H. Bau, "Feedback control to delay or advance linear loss of stability in planar Poiseuille flow," Proc. R. Soc. London, Ser. A **447**, 299 (1994).
[2] S. S. Joshi, J. L. Speyer, and J. Kim, "A systems theory approach to the feedback stabilization of infinitesimal and finite-amplitude disturbances in plane Poiseuille flow," J. Fluid Mech. **332**, 157 (1997).
[3] M. Gadel Hak, *Flow Control* (Cambridge University Press, Cambridge, 2000).
[4] T. R. Bewley and S. Liu, "Optimal and robust control and estimation of linear paths to transition," J. Fluid Mech. **365**, 305 (1998).
[5] T. R. Bewley, "Flow control: New challenges for a new renaissance," Prog. Aerosp. Sci. **37**, 21 (2001).
[6] D. T. J. Hurle, "Analytical representation of the shape of the meniscus in Czochralski growth," J. Cryst. Growth **63**, 13 (1983).
[7] E. Kuroda, H. Kozuka, and Y. Takano, "The effect of temperature oscillations at the growth interface on crystal perfection," J. Cryst. Growth **68**, 613 (1984).
[8] J. R. Carruthers, K. Prout, and F. J. C. Rossotti, "Structure and stability of carboxylate complexes," Acta Crystallogr., Sect. B: Struct. Crystallogr. Cryst. Chem. **31**, 2044 (1975).
[9] E. W. Müller, H. Spiering, and P. Gutlich, "Effect of crystal quality on the spin-transition behavior in a Cobalt (II) complex," Inorg. Chem. **23**, 119 (1984).
[10] J. Singer, Y-Z. Wang, and H. H. Bau, "Controlling a chaotic system," Phys. Rev. Lett. **66**, 1123 (1991).
[11] J. Singer and H. H. Bau, "Active control of convection," Phys. Fluids A **3**, 2859 (1991).
[12] Y-Z. Wang, J. Singer, and H. H. Bau, "Controlling chaos in a thermal convection loop," J. Fluid Mech. **237**, 479 (1992).
[13] J. A. Burns, B. B. King, and D. Rubio, "Feedback control of a thermal fluid using state estimation," Int. J. Comput. Fluid Dyn. **11**, 93 (1998).
[14] P. K. Yuen and H. H. Bau, "Rendering subcritical Hopf bifurcation supercritical," J. Fluid Mech. **317**, 91 (1996).
[15] P. K. Yuen and H. H. Bau, "Controlling chaotic convection using neural nets—theory and experiments," Neural Networks **11**, 557 (1998).
[16] P. K. Yuen and H. H. Bau, "Optimal and adaptive control of chaotic convection—theory and experiments," Phys. Fluids **11**, 1435 (1999).
[17] J. Tang and H. H. Bau, "Stabilization of the no-motion state in Rayleigh-Bénard convection through the use of feedback control," Phys. Rev. Lett. **70**, 1795 (1993).
[18] J. Tang and H. H. Bau, "Feedback control stabilization of the no-motion state of a fluid confined in a horizontal porous layer heated from below," J. Fluid Mech. **257**, 485 (1993).
[19] J. Tang and H. H. Bau, "Stabilization of the no-motion state in the Rayleigh-Bénard problem," Proc. R. Soc. London, Ser. A **447**, 587 (1994).
[20] J. Tang and H. H. Bau, "Stabilization of the no-motion state of a horizontal fluid layer heated from below with Joule Heating," J. Heat Transfer **117**, 329 (1995).
[21] J. Tang and H. H. Bau, "Experiments on the stabilization of the no-motion state of a fluid layer heated from below and cooled from above," J. Fluid Mech. **363**, 153 (1998).
[22] J. Tang and H. H. Bau, "Numerical investigation of the stabilization of the no-motion state of a fluid layer heated from below and cooled from above," Phys. Fluids **10**, 1597 (1998).
[23] L. E. Howle, "Linear stability analysis of controlled Rayleigh-Bénard convection using shadowgraphic measurement," Phys. Fluids **9**, 3111 (1997).
[24] L. E. Howle, "Control of Rayleigh—Bénard convection in a small aspect ratio container," Int. J. Heat Mass Transfer **40**, 817 (1997).
[25] L. E. Howle, "Active control of Rayleigh—Bénard convection," Phys. Fluids **9**, 1861 (1997).
[26] L. E. Howle, "The effect of boundary properties on controlled Rayleigh—Bénard convection," J. Fluid Mech. **411**, 39 (2000).
[27] T. A. Shortis and P. Hall, "On the effect of feedback control on Benard convection," NASA Contractor Report 198280, ICASE Report No. 96-9 (1996).
[28] A. C. Or, L. Cortelezzi, and J. L. Speyer, "Robust feedback control of Rayleigh-Bénard convection," J. Fluid Mech. **437**, 175 (2001).
[29] A. C. Or and J. L. Speyer, "Active suppression of finite-amplitude Rayleigh-Bénard convection," J. Fluid Mech. **483**, 111 (2003).
[30] L. N. Trefethen, "Pseudospectra of linear operators," SIAM Rev. **39**, 383 (1997).
[31] L. N. Trefethen, "Computation of pseudospectra," Acta Numerica **8**, 247 (1999).
[32] L. N. Trefethen, *Spectral Methods in Matlab* (SIAM, Philadelphia, 2000).
[33] L. N. Trefethen, A. E. Trefethen, S. C. Reddy, and T. A. Driscoll, "Hydrodynamic stability without eigenvalues," Science **261**, 578 (1993).
[34] J. Lim and J. Kim, 2004, "A singular value analysis of boundary layer control," Phys. Fluids **16**, 1980 (2004).
[35] E. Lauga, and T. Bewley, "The decay of stabilizability with Reynolds number in a linear model of spatially developing flows," Proc. R. Soc. London, Ser. A **459**, 2077 (2003).
[36] E. Lauga, and T. Bewley, "Performance of a linear robust control strategy on a nonlinear model of spatially-developing flows," J. Fluid Mech. **512**, 343 (2004).
[37] W. M. Deen, *Analysis of Transport Phenomena* (Oxford University Press, Oxford, 1998).
[38] K. H. Huebner and E. A. Thornton, *The Finite Element Method for Engineers* (Wiley, New York, 1982).
[39] L. J. Segerlind, *Applied Finite Element Analysis* (Wiley, New York, 1976).
[40] D. A. S. Rees, "The stability of Darcy-Benard Convection," in *Handbook of Porous Media*, edited by K. Vafai (Dekker, New York, 2000).
[41] J. B. Burl, *Linear Optimal Control* (Addison-Wesley, Boston, MA, 1999).
[42] K. M. Butler and B. F. Farrell, "Optimal perturbations and streak spacing in wall-bounded turbulent shear flow," Phys. Fluids A **5**, 774 (1993).
[43] P. R. Spalart, R. D. Moser, and M. M. Rogers, "Spectral methods for the Navier-Stokes equations with one infinite and two periodic directions," J. Comput. Phys. **96**, 297 (1991).
[44] J. F. Wildborne, J. McKernan, and A. J. Steer, "On minimizing maximum transient energy growth," College of Aeronautics Report No. 0501, Cranfied University (2005).